ACS Medicinal Chemistry Letters

pubs.acs.org/acsmedchemlett Letter

Discovery of PIPE-359, a Brain-Penetrant, Selective M_1 Receptor Antagonist with Robust Efficacy in Murine MOG-EAE

Thomas O. Schrader,*,† Yifeng Xiong,† Ariana O. Lorenzana, Alexander Broadhead, Karin J. Stebbins, Michael M. Poon, Christopher Baccei, and Daniel S. Lorrain

Cite This: *ACS Med. Chem. Lett.* 2021, 12, 155−161

Read Online

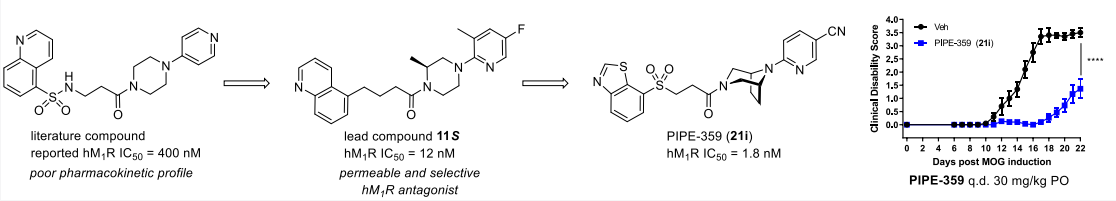

ABSTRACT: The discovery of PIPE-359, a brain-penetrant and selective antagonist of the muscarinic acetylcholine receptor subtype 1 is described. Starting from a literature-reported M_1 antagonist, linker replacement and structure−activity relationship investigations of the eastern 1-(pyridinyl)piperazine led to the identification of a novel, potent, and selective antagonist with good MDCKII-MDR1 permeability. Continued semi-iterative positional scanning facilitated improvements in the metabolic and hERG profiles, which ultimately delivered PIPE-359. This advanced drug candidate exhibited robust efficacy in mouse myelin oligodendrocyte glycoprotein (MOG)-induced experimental autoimmune encephalitis (EAE), a preclinical model for multiple sclerosis.

KEYWORDS: *M_1-selective, antimuscarinic, M_1 antagonist, EAE, remyelination*

Multiple sclerosis (MS) is an immune-mediated disorder characterized by destruction of the insulating myelin that surrounds the axons of neurons in the central nervous system (CNS).[1−3] The result of demyelination is an impairment of conduction along the affected nerve, which can manifest itself in a variety of neurological symptoms from mild to severe. A 2017 study[4] estimated that nearly 1 million individuals in the U.S. are living with MS. Fortunately, there have been tremendous breakthroughs in pharmacotherapies for the treatment of MS in the last few decades.[5,6] A vast majority of these drugs dampen the peripheral immune response, resulting in the reduction of relapses and the delay of overall progression of disabilities.[7] However, a true "cure", which would require the repair and restoration of nerve function, is not currently available.

Remyelination represents an attractive avenue to facilitate repair of nerve function within the CNS in patients diagnosed with MS.[8] Remyelination involves differentiation of oligodendrocyte progenitor cells (OPCs) into mature oligodendrocytes,[9] the neuroglia responsible for creating the myelin sheath. High-throughput screening efforts have identified nonselective antimuscarinics as myelin-regenerative compounds.[10,11] Subsequently benztropine (Figure 1), a CNS-penetrant antimuscarinic, and clemastine, an antihistamine that possesses anticholinergic activity, have both demonstrated efficacy in mouse myelin oligodendrocyte glycoprotein (MOG)-induced experimental autoimmune encephalitis (MOG-EAE),[10,12] a widely used preclinical model for multiple sclerosis. As a reduction in clinical score in EAE can be attributed to either an immunomodulatory effect, remyelination, or some combination thereof, Chan and co-workers used M_1 muscarinic receptor (M_1R) knockout mice to demonstrate that remyelination itself is sufficient.[12] Additional support for the M_1R as a target for remyelination is provided by the phase II ReBUILD trial, where clemastine fumarate showed encouraging results in promoting visual-pathway remyelination in patients with MS as

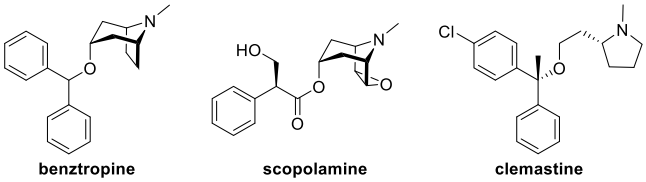

Figure 1. Structures of the nonselective antimuscarinics benztropine and scopolamine and the mixed antihistamine−antimuscarinic clemastine.

Received: November 27, 2020
Accepted: December 22, 2020
Published: December 24, 2020

determined by reduced visual-evoked potential (VEP) P100 latency as the primary outcome measure.[13] The effect is thought to be the result of off-target antagonism of muscarinic receptors.[12,14] Taken together, these results show that selective M_1R antagonism represents a truly differentiated approach to the treatment of MS through remyelination. Accordingly, details of the discovery of a CNS-penetrant M_1R antagonist, PIPE-359, are provided herein.

There are five subtypes (M_1−M_5) of muscarinic acetylcholine receptors (mAChRs), a subclass of G-protein-coupled receptors (GPCRs), which are widely distributed to varying degrees in the CNS and periphery that elicit a diverse range of biological functions.[15] The orthosteric binding site is highly conserved across all five subtypes,[16] and consequently, very few selective small-molecule M_1R antagonists have been identified to date.[17−20] Conversely, there are myriad nonselective antagonists, many of which are FDA-approved medications.[21] Commonly prescribed antimuscarinics include benztropine (Cogentin) for symptoms of Parkinson's disease, tiotropium (Spiriva) for chronic obstructive pulmonary disease (COPD) or asthma, and oxybutynin (Ditropan) for overactive bladder (OAB). Despite the prevalence of pan-antimuscarinics, a selective M_1R antagonist is desirable to reduce unwanted side effects associated with nonselective compounds.[21,22] For example, the selective M_1R antagonist VU0255035 (Figure 2) demonstrated inhibition of pilocarpine-induced seizures in

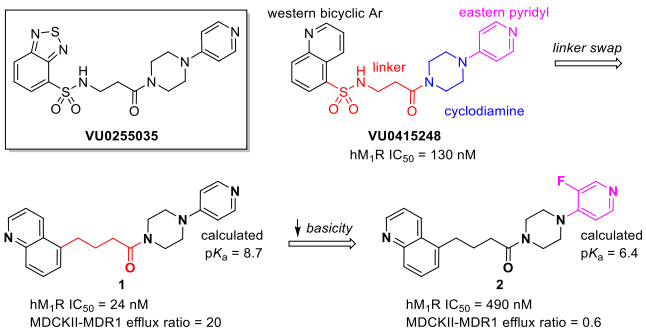

Figure 2. M_1R-selective antagonist VU0255035 and initial SAR development from VU0415248.

mice at 10 mg/kg ip but did not result in the cognitive impairment observed with the nonselective M_1R antagonist scopolamine in a hippocampus-dependent learning model.[17] A related molecule, VU0415248,[18] served as the starting point for our structure−activity relationship (SAR) study.

A structural breakdown of VU0415248 is shown in Figure 2. As the target is a centrally expressed M_1R, we initially focused on replacing the sulfonamide linker with a less polar carbon-based linker, a design element intended to facilitate brain permeation, as topological polar surface area (tPSA) and hydrogen-bond donor (HBD) count are known to negatively correlate with brain exposure.[23−25] Direct replacement of the sulfonamide group of VU0415248 with a methylene unit gave compound **1**, which came with a surprising 5-fold increase in antagonist potency on the human M_1R (hM_1R). Despite the decrease in tPSA and lack of an HBD, compound **1** suffered from considerable PgP-mediated efflux in the MDCKII-MDR1 permeability assay,[26] likely due to the presence of a highly basic eastern pyridyl ring. Lessening of the basicity by the addition of a fluorine atom (compound **2**) significantly reduced the efflux but unfortunately came with a cost in potency.

To identify a viable lead with appreciable potency and minimal PgP efflux, a small library of weakly basic (calculated $pK_a \leq 7$)[27] analogues (**3**−**17**) were synthesized by coupling readily available monopyridinyl cyclodiamines with 4-(quinolin-5-yl)butanoic acid. Human M_1R IC_{50} values are shown in Table 1. IC_{50} values ranging from 6.3 to 69 nM were observed

Table 1. IC_{50}[a] and pIC_{50} Values for Various 4-(Quinolin-5-yl)butanoic Amide Analogues

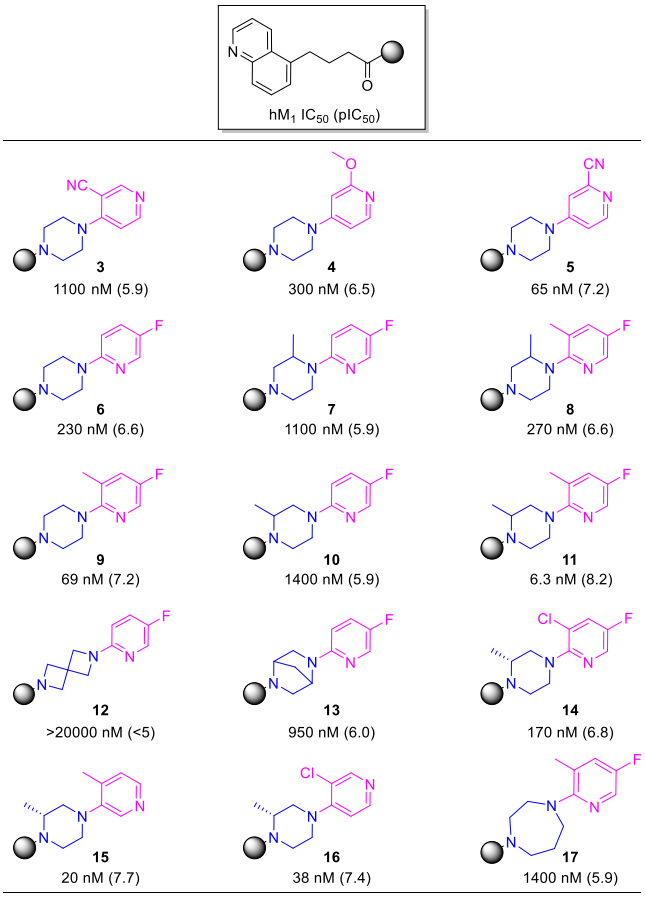

[a]IC_{50} values were taken as dose-dependent decreases in the EC_{80} acetylcholine response determined in CHO-K1 cells expressing the hM_1R.

for compounds **5**, **9**, **11**, **15**, and **16**, indicating that a strongly basic nitrogen atom was not required for potency. Potency was achieved with the pyridyl nitrogen either ortho (**9** and **11**), meta (**15**), or para (**5** and **16**) to the piperazine substitution. Replacing the piperazine with a 2,6-diazaspiro[3.3]heptane (**12** vs **6**), 2,5-diazabicyclo[2.2.1]heptane (**13** vs **6**), or homopiperazine (**17** vs **9**) decreased the potency. Comparisons of 1-(5-fluoropyridin-2-yl)piperazine amide **6** with analogues that possessed methyl substitutions on the piperazine ring (**7** and **10**) revealed potency losses of roughly half an order of magnitude. However, potency increases were observed when a methyl group was added to the fluoropyridine ring ortho to the piperazine substitution (**9** vs **6**, **8** vs **7**, and **11** vs **10**). In fact, "magic dimethyl" analogue **11** (IC_{50} = 6.3 nM) was approximately 40-fold, 10-fold, and 200-fold more potent than the desmethyl (**6**), methylpyridyl (**9**), and methylpipera-

https://dx.doi.org/10.1021/acsmedchemlett.0c00626
ACS Med. Chem. Lett. 2021, 12, 155−161

zyl (**10**) analogues, respectively. The enantiomers of compound **11** were synthesized individually, and their functional activities, measured across the human M_{1-4} receptors, are shown in Table 2. In-house data for benztropine

Table 2. Human Muscarinic Receptor (hM_nR) Functional Potencies (pIC_{50}) and Selectivities (ΔpIC_{50}) for Compounds 11*R*, 11*S*, and Benztropine

compd	hM_n pIC_{50} ($\Delta pIC_{50}[M_1 - M_n]$)			
	M_1	M_2	M_3	M_4
11*R*	8.2	6.2 (2.0)	6.3 (1.9)	7.4 (0.8)
11*S*	7.9	5.7 (2.2)	5.9 (2.0)	6.6 (1.3)
benztropine	8.6	7.2 (1.4)	7.7 (0.9)	8.3 (0.3)

are included for reference. Both enantiomers **11***R* and **11***S* were potent antagonists of the hM_1R and exhibited selectivities superior to that of benztropine. Excellent selectivities (>75-fold) versus the hM_2 and hM_3 receptors were observed, and the *S* isomer (**11***S*) displayed better selectivity versus the hM_4R (ΔpEC_{50} = 1.3) than did the *R* isomer (**11***R*) (ΔpEC_{50} = 0.8). On the basis of the activity and selectivity profile of **11***S*, the compound was selected for profiling in the MDCKII-MDR1 assay, which revealed good permeability (8.0×10^{-6} cm/s) and low PgP-mediated efflux (efflux ratio = 0.5). Further optimizations would be based on this promising early lead (**11***S*).

While a desirable level of hM_1R potency was achieved with a number of 4-(quinolin-5-yl)butanoic amides, selected compounds **5**, **9**, **11**, **15**, and **16** all lacked metabolic stability when incubated in rat liver microsomes (<1% parent remaining after 15 min of incubation). An initial attempt to improve the metabolic stability involved decreasing the overall lipophilicity[28] of the molecule via replacement of the quinoline ring. A series of carbon-based amide analogues were designed in which the western bicyclic heteroarene contained a ring nitrogen atom in a similar or adjacent position to that of the quinoline,[18] while the eastern end of the scaffold was fixed as the (*S*)-1-(5-fluoro-3-methylpyridin-2-yl)-3-methylpiperazine of compound **11***S*. Results are shown in Table 3. The less lipophilic quinazoline **18a** and hydroxymethyl quinoline **18c** were less potent (83 and 170 nM, respectively) than compound **11***S* and failed to significantly improve the metabolic stability versus **11***S* in rat liver microsome incubations. While not less lipophilic (as calculated) than **11***S*, the moderately potent benzo[*d*]thiazole **18d** displayed a >25-fold increase in stability. Adding an additional amino substituent to the benzo[*d*]thiazole (compound **18e**) or swapping the sulfur atom for an oxygen (benzo[*d*]oxazole **18f**) did not further improve the stability.

Although benzo[*d*]thiazole **18d** had increased metabolic stability versus **11***S* in vitro, the improvement was not significant enough to warrant further in vivo profiling. Attention subsequently turned toward modification of the linker. Based on **18d**, a limited scan of more polar heteroatom-containing linkers was performed. Of the four linker variants shown in Table 4, only **19c** containing a 3-sulfonylamide linker retained appreciable potency. While introduction of the sulfone functionality further protected the scaffold from oxidative metabolism (vs **18d**), further optimization was necessary.

At this point in our discovery program, reoptimization of the eastern 1-(pyridinyl)cyclodiamine end of the molecule was carried out while fixing the western aromatic and linker as the more stable 3-(benzo[*d*]thiazol-7-ylsulfonyl)propanamide. An emphasis was placed on designing compounds with logD

Table 3. Positional Scan of the Western Bicyclic Heteroarene

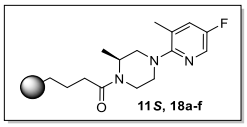

Cmpd	hM_1R IC_{50} (pIC_{50})	calcd. logD[a]	rMS %@15min[b]
 **11 S**	13 nM (7.9)	4.5	0.2%
 **18a**	83 nM (7.1)	3.8	0.0%
 **18b**	>20 μM (<5)	3.8	n.d.
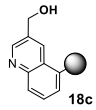 **18c**	170 nM (6.8)	3.7	1.0%
 **18d**	24 nM (7.6)	4.5	5.3%
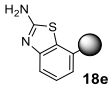 **18e**	190 nM (6.7)	4.3	3.7%
 **18f**	230 nM (6.6)	3.7	0.0%

[a]Calculated for pH 7.4 using the ChemAxon logD plugin. [b]Percentage of parent compound remaining after 15 min of incubation (at 1 μM initial concentration) in rat liver microsomes (0.5 mg/mL).

Table 4. Positional Scan of Heteroatom-Containing Linkers

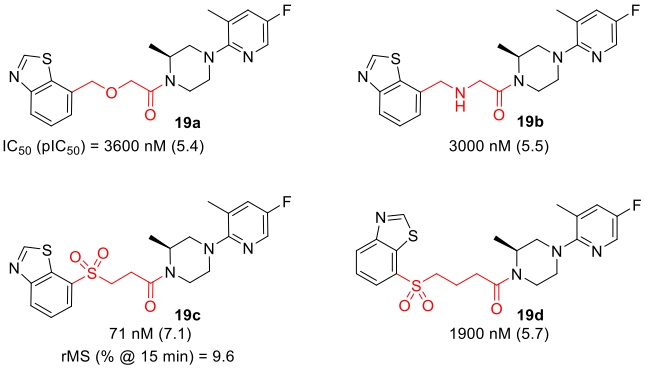

https://dx.doi.org/10.1021/acsmedchemlett.0c00626
ACS Med. Chem. Lett. 2021, 12, 155−161

values significantly lower than that of sulfone **19c** (calcd logD = 2.7). In this vein, we initially limited the cyclodiamine core to the less lipophilic unsubstituted piperazine. Coupling of several 1-(pyridinyl)piperazines with 3-(benzo[*d*]thiazol-7-ylsulfonyl)propanoic acid produced derivatives **20a–h** shown in Table 5. Better potencies were achieved when the pyridine

Table 5. Positional Scan of the Eastern Pyridyl

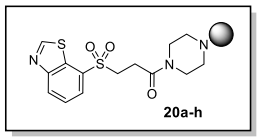

Cmpd	hM$_1$R IC$_{50}$ (pIC$_{50}$)	calcd. logD	rMS %@ 15min
 **20a**	380 nM (6.4)	1.1	29%
 **20b**	8500 nM (5.1)	1.8	n.d.
 **20c**	4800 nM (5.3)	2.2	n.d.
 **20d**	440 nM (6.4)	1.2	n.d.
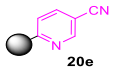 **20e**	5.8 nM (8.2)	1.4	59%
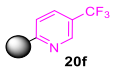 **20f**	32 nM (7.5)	2.5	41%
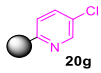 **20g**	160 nM (6.8)	2.2	31%
 **20h**	260 nM (6.6)	1.5	n.d.

nitrogen atom was ortho to the piperazine substitution (compounds **20e–g**) versus being meta (**20h**) or para (**20a–d**). Of particular note, nicotinonitrile **20e** (IC$_{50}$ = 5.8 nM) exhibited potency on par with the most potent compound (**11***R*, IC$_{50}$ = 6.3 nM) in the carbon-based series. Additionally, **20e** was found to be considerably more stable in rat liver microsome incubations (59% parent remaining at 15 min) compared with the initial sulfone lead **19c** (9.6% remaining at 15 min). For this reason, **20e** was selected for further profiling in vivo. At 2 h after oral dose (10 mg/kg), the average unbound plasma and brain concentrations in rats (n = 2) of **20e** were 13 and 2.2 nM, respectively (Table 6). The presence of free **20e** in the rat CNS after oral administration at a concentration approaching its in vitro functional potency

Table 6. Rat NeuroPK and hERG Inhibition Data for Compound 20e

compd	C_p (nM)	$f_{u,p}$	$C_{p,u}$ (nM)	$C_{b,u}$ (nM)	$K_{p,uu}$	hERG @ 3 μM
20e	89	0.15	13	2.2	0.17	69%

prompted us to assess M$_1$R engagement in vivo. Unfortunately, a preliminary receptor occupancy experiment[29] performed in mice gave underwhelming results, as a 30 mg/kg po dose achieved only ∼50% receptor occupancy at 2 h, suggesting that the compound would be unsuitable for evaluation in the EAE model. In addition, further characterization of **20e** revealed a potential hERG liability (69% inhibition at 3 μM).

The next set of optimizations involved fixing the niconitrile and western 3-(benzo[*d*]thiazol-7-ylsulfonyl)propanamide sections of **20e** and performing a scan of the piperazine core (Table 7). The goal was to achieve improvements in PK and/

Table 7. Positional Scan of the Central Azacycle

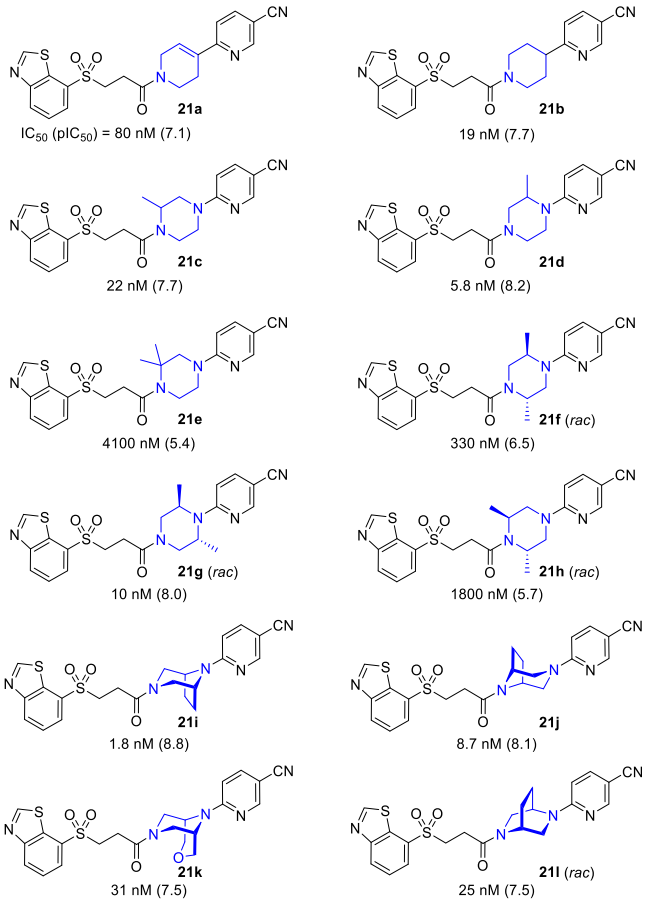

or M$_1$R potency, either of which should translate into increased M$_1$R occupancy in vivo. To improve brain permeation via the reduction of polar surface area, tetrahydropyridine **21a** and piperidine **21b** were prepared. Unfortunately, both **21a** (80 nM) and **21b** (19 nM) had decreased potencies compared with **20e** (5.8 nM). Methylation of the piperazine ring was preferred closer to the cyanopyridine (**21d** vs **21c**), and potency was maintained with an additional methyl substitution on the piperazine ring (**21g**), but only when it was placed adjacent to the anilinic nitrogen (**21g** vs **21f**). When two methyl groups were placed adjacent to the amide nitrogen

https://dx.doi.org/10.1021/acsmedchemlett.0c00626
ACS Med. Chem. Lett. 2021, 12, 155−161

atom of the piperazine (compounds **21e** and **21h**), the potency dropped significantly. Also included in the scan were bridged bicyclic variants **21i–l**, all of which exhibited reasonable hM_1R antagonism. Comparison of symmetrical azatropanes **21i** (IC_{50} = 1.8 nM) and **21j** (IC_{50} = 8.7 nM) revealed a preference for the bridge to be proximal to the cyanopyridine, similar to the SAR observed with dimethylated analogues **21g** and **21h**. Gratifyingly, readouts for potent azatropane **21i** in both rat microsomal stability (67% remaining at 15 min) and hERG inhibition (36% inhibition at 3 μM) revealed improvements versus **20e**.

Further profiling of compound **21i**, designated as PIPE-359, was carried out, and the results are shown in Table 8. Radioligand binding affinity (K_i) measurements with [^{3}H]-*N*-methyl scopolamine revealed exceptionally high affinity for the hM_1R (K_i = 0.14 nM). Furthermore, PIPE-359 exhibited good-to-excellent selectivities versus the hM_2R, hM_3R, and hM_4R in both functional and binding[30] settings. PIPE-359 had moderate intrinsic clearance when incubated with both rat and mouse liver microsomes (extraction ratios of 0.42 and 0.47, respectively). In rat PK (2/10 mg/kg iv/po), a total clearance of 56 mL min^{-1} kg^{-1} was observed, along with an oral bioavailability of 4.5%. More importantly, an unbound brain concentration ($C_{b,u}$) of 3.4 nM was reached 2 h after 10 mg/kg oral administration of PIPE-359, a concentration several fold over the measured hM_1R K_i.

To assess the candidacy and dosing regimen of PIPE-359 in the MOG-EAE model, mouse M_1R occupancy studies were performed (Figure 3). In an initial experiment, PIPE-359 was dosed orally at 0.1, 1.0, 10, and 30 mg/kg (n = 3/group). At 2 h, a dose-dependent increase in M_1R occupancy was observed, with full occupancy achieved at 30 mg/kg (Figure 3a). A follow-up time-course M_1R occupancy study with a 30 mg/kg po dose of PIPE-359 revealed that full receptor occupancy was maintained for up to 8 h (Figure 3b) with a drop to 40% occupancy at 24 h. Bioanalysis of the 8 h plasma and forebrain concentrations of PIPE-359 revealed an average unbound plasma concentration ($C_{p,u}$) of 117 nM and an average $C_{b,u}$ of 4.9 nM (8 h $K_{p,uu}$ = 0.04), the latter being well above the functional potency (IC_{50} = 1.8 nM) and binding affinity (K_i = 0.14 nM) of PIPE-359. While the 24 h brain concentrations of PIPE-359 were below the limit of quantification, extrapolation from the average unbound plasma concentration ($C_{p,u}$ at 24 h = 2.9 nM) using a $K_{p,uu}$ value of 0.04 yields a $C_{b,u}$ at 24 h of 0.12 nM, a value consistent with the 40% occupancy observed. On the basis of these results, PIPE-359 was evaluated in the mouse MOG-EAE model by dosing orally qd at 30 mg/kg. As

Table 8. Profile of PIPE-359 (21i)

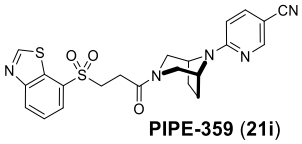

PIPE-359 (21i)

Human mAChR Activity	
IC_{50} (pIC_{50})	$\Delta pIC_{50}[M_1 - M_n]$
M_1: 1.8 nM (8.8)	
M_2: 200 nM (6.7)	2.1
M_3: 55 nM (7.3)	1.5
M_4: 22 nM (7.7)	1.1
K_i (pK_i)	$\Delta pK_i[M_1 - M_n]$
M_1: 0.14 nM (9.8)	
M_2: 19 nM (7.7)	2.1
M_3: 0.84 nM (9.1)	0.7
M_4: 6.5 nM (8.2)	1.6
In Vitro ADMET	
microsomal stability	
Cl_{int} (μL/min/mg): 42 (human), 23 (rat), 21 (mouse)	
predicted extraction ratio: 0.72 (h), 0.42 (r), 0.47 (m)	
tissue binding	
PPB f_u: 0.20 (r), 0.18 (m)	
BTB f_u: 0.13 (m)	
MDCK-MDR1 permeability	
P_{app} (A-B): 7.7 × 10^{-6} cm/s	
efflux ratio: 3.9	
hERG inhibition (patch clamp)	
IC_{50}: 5.6 μM	
CYP inhibition	
IC_{50}: > 10 μM (2C9, 2D6, 3A4)	
Rat PK	
iv/po 2/10 mg/kg	
Cl/Cl_u: 56/273 mL min^{-1} kg^{-1}	
$t_{1/2}$ (iv): 0.9 h	
AUC/AUC_u: 100/21 h ng/mL	
F: 4.5%	
NeuroPK 10 mg/kg po 2 h after dose	
$C_b/C_{b,u}$: 26/3.4 nM	
$C_p/C_{p,u}$: 80/16 nM	
$K_p/K_{p,uu}$: 0.33/0.21	

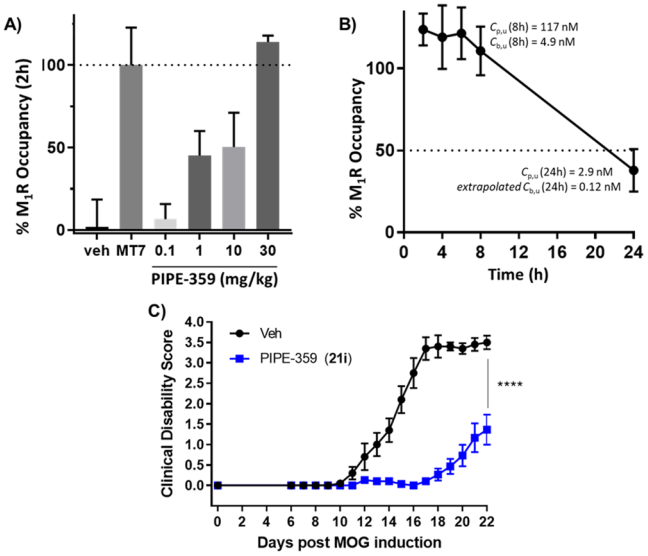

Figure 3. Mouse receptor occupancy and MOG-EAE experiments with PIPE-359 (**21i**). (A) Dose–response receptor occupancy 2 h after po dose. [^{3}H]-Pirenzepine (300 nM) was added ex vivo as a radiotracer. Occupancy was measured as % response of hM_1R-selective antagonist muscarinic toxin 7 (MT7)[31] added ex vivo (300 nM). (B) Receptor occupancy time course of PIPE-359 at 30 mg/kg po. (C) Prophylactic treatment (qd 30 mg/kg po) with PIPE-359 in MOG-EAE performed in C57BL/6 mice (n = 10–15/group). EAE induction was performed on day 0 followed by once daily administration (qd) of PIPE-359 at 30 mg/kg po or vehicle for 21 days. Clinical scores were recorded daily, and changes were observed starting on day 6 and continued through day 22. ****, $p < 0.0001$ based on Sidak's multiple comparison tests respective to vehicle controls.

https://dx.doi.org/10.1021/acsmedchemlett.0c00626
ACS Med. Chem. Lett. 2021, 12, 155–161

shown in Figure 3c, separation of clinical scores between drug- and vehicle-treated animals emerged on day 11, increased through to the peak of disease (day 17), and persisted throughout the chronic phase of the study. To our knowledge, this is the first demonstration of efficacy in EAE with a selective M_1R antagonist.

In summary, PIPE-359 (**21i**), a brain-penetrant and selective hM_1R antagonist with remarkable efficacy in mouse MOG-EAE was discovered. A first round of optimization from a known weakly active hM_1R-selective antagonist delivered a permeable, potent, and selective molecule (compound **11***S*). Subsequent rounds of positional scanning improved the pharmacokinetics and hERG liabilities, ultimately delivering PIPE-359. The demonstration of efficacy with PIPE-359 in EAE provides a path forward for the use of selective hM_1R antagonists as treatments for MS patients. Continued optimizations, which involve improving target selectivity and brain permeation, are ongoing and will be reported in due course.

■ ASSOCIATED CONTENT

Supporting Information

The Supporting Information is available free of charge at https://pubs.acs.org/doi/10.1021/acsmedchemlett.0c00626.

Conditions for in vitro biological assays, in vitro ADMET assays, synthetic procedures, analytical data for all compounds, and full characterization data for compounds **11***S*, **20e**, and **21i** (PDF)

■ AUTHOR INFORMATION

Corresponding Author

Thomas O. Schrader − *Pipeline Therapeutics, San Diego, California 92121, United States;* orcid.org/0000-0003-3468-9566; Email: tschrader@pipeline-tx.com

Authors

Yifeng Xiong − *Pipeline Therapeutics, San Diego, California 92121, United States*

Ariana O. Lorenzana − *Pipeline Therapeutics, San Diego, California 92121, United States*

Alexander Broadhead − *Pipeline Therapeutics, San Diego, California 92121, United States*

Karin J. Stebbins − *Pipeline Therapeutics, San Diego, California 92121, United States*

Michael M. Poon − *Pipeline Therapeutics, San Diego, California 92121, United States*

Christopher Baccei − *Pipeline Therapeutics, San Diego, California 92121, United States*

Daniel S. Lorrain − *Pipeline Therapeutics, San Diego, California 92121, United States*

Complete contact information is available at: https://pubs.acs.org/10.1021/acsmedchemlett.0c00626

Author Contributions

[†]T.O.S. and Y.X. contributed equally. The manuscript was written through contributions of all authors. All of the authors approved the final version of the manuscript.

Notes

The authors declare no competing financial interest.

■ ACKNOWLEDGMENTS

The authors thank Yunlong Yang (WuXi AppTec), Yu Xue (Pharmaron, Inc.), and their colleagues for synthetic contributions, and Danxi Li (Pharmaron, Inc.) and her colleagues for providing in vitro ADMET data. We also thank John Frazer (Beacon Discovery) for providing radioligand binding data for compound **21i**.

■ ABBREVIATIONS

MS, multiple sclerosis; MOG-EAE, myelin oligodendrocyte glycoprotein-induced experimental autoimmune encephalitis; CNS, central nervous system; OPC, oligodendrocyte progenitor cell; VEP, visual-evoked potential; M_1R, muscarinic receptor subtype 1; mAChR, muscarinic acetylcholine receptor; GPCR, G-protein-coupled receptor; CHO, Chinese hamster ovary; rMS, rat microsomal stability; PgP, P-glycoprotein 1; MDCKII-MDR1, Madin-Darby canine kidney II-multidrug resistance protein; PK, pharmacokinetic; ADMET, absorption, distribution, metabolism, excretion, and toxicity; ip, intraperitoneal; po, per os (oral); iv, intravenous; qd, quaque die (once daily); SAR, structure−activity relationship; HBD, hydrogen-bond donor; tPSA, topological polar surface area; PPB, plasma protein binding; f_u, fraction unbound; BTB, brain tissue binding; $C_{b,u}$, unbound brain concentration; $C_{p,u}$, unbound plasma concentration; $K_{p,uu}$, ratio of unbound brain compound concentration to unbound plasma compound concentration; hERG, human ether-à-go-go-related gene; CYP, cytochrome P450.

■ REFERENCES

(1) Lemus, H. N.; Warrington, A. E.; Rodriguez, M. Multiple Sclerosis: Mechanisms of Disease and Strategies for Myelin and Axonal Repair. *Neurol. Clin.* **2018**, *36*, 1−11.

(2) Frohman, E. M.; Racke, M. K.; Raine, C. S. Multiple Sclerosis-The Plaque and Its Pathogenesis. *N. Engl. J. Med.* **2006**, *354*, 942−955.

(3) National Multiple Sclerosis Society. *What Is MS?* https://www.nationalmssociety.org/What-is-MS (accessed 2020-12-10).

(4) Wallin, M. T.; Culpepper, W. J.; Campbell, J. D.; Nelson, L. M.; Langer-Gould, A.; Marrie, R. A.; Cutter, G. R.; Kaye, W. E.; Wagner, L.; Tremlett, H.; Buka, S. L.; Dilokthornsakul, P.; Topol, B.; Chen, L. H.; LaRocca, N. G. The prevalence of MS in the United States: A population-based estimate using health claims data. *Neurology* **2019**, *92*, e1029−e1040.

(5) Costello, K.; Halper, J.; Kalb, R.; Skutnik, L.; Rapp, R. *The Use of Disease-Modifying Therapies in Multiple Sclerosis: Principles and Current Evidence*. A Consensus Paper by the Multiple Sclerosis Coalition, updated September 2019. https://www.nationalmssociety.org/NationalMSSociety/media/MSNationalFiles/Brochures/DMT_Consensus_MS_Coalition.pdf (accessed 2020-12-10).

(6) Goldschmidt, C.; McGinley, M. P. Advances in the Treatment of Multiple Sclerosis. *Neurol. Clin.* **2021**, *39*, 21−33.

(7) Rommer, P. S.; Milo, R.; Han, M. H.; Satyanarayan, S.; Sellner, J.; Hauer, L.; Illes, Z.; Warnke, C.; Laurent, S.; Weber, M. S.; Zhang, Y.; Stuve, O. Immunological aspects of approved MS therapeutics. *Front. Immunol.* **2019**, *10*, 1564.

(8) Baldassari, L. E.; Feng, J.; Clayton, B. L. L.; Oh, S.-H.; Sakaie, K.; Tesar, P. J.; Wang, Y.; Cohen, J. A. Developing therapeutic strategies to promote myelin repair in multiple sclerosis. *Expert Rev. Neurother.* **2019**, *19*, 997−1013.

(9) Emery, B. Regulation of oligodendrocyte differentiation and myelination. *Science* **2010**, *330*, 779−782.

(10) Deshmukh, V.; Tardif, V.; Lyssiotis, C. A.; Green, C. C.; Kerman, B.; Kim, H. J.; Padmanabhan, K.; Swoboda, J. G.; Ahmad, I.; Kondo, T.; Gage, F. H.; Theofilopoulos, A. N.; Lawson, B. R.; Schultz,

P. G.; Lairson, L. L. A regenerative approach to the treatment of multiple sclerosis. *Nature* **2013**, *502*, 327−332.

(11) Mei, F.; Fancy, S. P. J.; Shen, Y. A.; Niu, J.; Zhao, C.; Presley, B.; Miao, E.; Lee, S.; Mayoral, S. R.; Redmond, S. A.; Etxeberria, A.; Xiao, L.; Franklin, R. J. M.; Green, A.; Hauser, S. L.; Chan, J. R. Micropillar arrays as a high-throughput screening platform for therapeutics in multiple sclerosis. *Nat. Med.* **2014**, *20*, 954−960.

(12) Mei, F.; Lehmann-Horn, K.; Shen, Y. A.; Rankin, K. A.; Stebbins, K. J.; Lorrain, D. S.; Pekarek, K.; Sagan, S. A.; Xiao, L.; Teuscher, C.; von Büdingen, H.-C.; Wess, J.; Lawrence, J. J.; Green, A. J.; Fancy, S. J. P.; Zamvil, S. S.; Chan, J. R. Accelerated remyelination during inflammatory demyelination prevents axonal loss and improves functional recovery. *eLife* **2016**, *5*, No. e18246.

(13) Green, A. J.; Gelfand, J. M.; Cree, B. A.; Bevan, C.; Boscardin, W. J.; Mei, F.; Inman, J.; Arnow, S.; Devereux, M.; Abounasr, A.; Nobuta, H.; Zhu, A.; Friessen, M.; Gerona, R.; von Büdingen, H. C.; Henry, R. G.; Hauser, S. L.; Chan, J. R. Clemastine fumarate as a remyelinating therapy for multiple sclerosis (ReBUILD): a randomised, controlled, double-blind, crossover trial. *Lancet* **2017**, *390*, 2481−2489.

(14) Tesar, P. J.; Cohen, J. A. Clemastine fumarate for promotion of optic nerve remyelination. *Lancet* **2017**, *390*, 2421−2422.

(15) *Muscarinic Receptors*; Fryer, A. D., Christopoulos, A., Nathanson, N. M., Eds.; Handbook of Experimental Pharmacology, Vol. *208*; Springer: Berlin, 2012.

(16) Thal, D. M.; Sun, B.; Feng, D.; Nawaratne, V.; Leach, K.; Felder, C. C.; Bures, M. G.; Evans, D. A.; Weis, W. I.; Bachhawat, P.; Kobilka, T. S.; Sexton, P. M.; Kobilka, P. K.; Christopoulos, A. Crystal structures of the M1 and M4 muscarinic acetylcholine receptors. *Nature* **2016**, *531*, 335−340.

(17) Sheffler, D. J.; Williams, R.; Bridges, T. M.; Xiang, Z.; Kane, A. S.; Byun, N. E.; Jadhav, S.; Mock, M. M.; Zheng, F.; Lewis, L. M.; Jones, C. K.; Niswender, C. M.; Weaver, C. D.; Lindsley, C. W.; Conn, P. J. A Novel Selective Muscarinic Acetylcholine Receptor Subtype 1 Antagonist Reduces Seizures without Impairing Hippocampus-Dependent Learning. *Mol. Pharmacol.* **2009**, *76*, 356−368.

(18) Melancon, B. J.; Lamers, A. P.; Bridges, T. M.; Sulikowski, G. A.; Utley, T. J.; Sheffler, D. J.; Noetzel, M. J.; Morrison, R. D.; Daniels, J. S.; Niswender, C. M.; Jones, C. K.; Conn, P. J.; Lindsley, C. W.; Wood, M. R. Development of a more highly selective M_1 antagonist from the continued optimization of the MLPCN Probe ML012. *Bioorg. Med. Chem. Lett.* **2012**, *22*, 1044−1048.

(19) Melancon, B. J.; Utley, T. J.; Sevel, C.; Mattmann, M. E.; Cheung, Y.-Y.; Bridges, T. M.; Morrison, R. D.; Sheffler, D. J.; Niswender, C. M.; Daniels, J. S.; Conn, P. J.; Lindsley, C. W.; Wood, M. R. Development of novel M_1 antagonist scaffolds through the continued optimization of the MLPCN probe ML012. *Bioorg. Med. Chem. Lett.* **2012**, *22*, 5035−5040.

(20) Miller, N. R.; Daniels, R. N.; Lee, P.; Conn, P. J.; Lindsley, C. W. Synthesis and SAR of *N*-(4-(4-alklylpiperazin-1-yl)phenyl)-benzamides as muscarinic acetylcholine receptor subtype 1 (M_1) antagonists. *Bioorg. Med. Chem. Lett.* **2010**, *20*, 2174−2177.

(21) Chew, M. L.; Mulsant, B. H.; Pollock, B. G.; Lehman, M. E.; Greenspan, A.; Mahmoud, R. A.; Kirshner, M. A.; Sorisio, D. A.; Bies, R. R.; Gharabawi, G. Anticholinergic activity of 107 medications commonly used by older adults. *J. Am. Geriatr. Soc.* **2008**, *56*, 1333−1341.

(22) Wagg, A.; Verdejo, C.; Molander, U. Review of cognitive impairment with antimuscarinic agents in elderly patients with overactive bladder. *Int. J. Clin. Pract.* **2010**, *64*, 1279−1286.

(23) Dichiara, M.; Amata, B.; Turnaturi, R.; Marrazzo, A.; Amata, E. Tuning Properties for Blood−Brain Barrier (BBB) Permeation: A Statistics-Based Analysis. *ACS Chem. Neurosci.* **2020**, *11*, 34−44.

(24) Gupta, M.; Lee, H.-J.; Barden, C. J.; Weaver, D. F. The Blood−Brain Barrier (BBB) Score. *J. Med. Chem.* **2019**, *62*, 9824−9836.

(25) Wager, T. T.; Hou, X.; Verhoest, P. R.; Villalobos, A. Moving Beyond Rules: The Development of a Central Nervous System Multiparameter Optimization (CNS MPO) Approach to Enable Alignment of Druglike Properties. *ACS Chem. Neurosci.* **2010**, *1*, 435−449.

(26) The MDR1-MDCKII cell line was obtained from The Netherlands Cancer Institute (Amsterdam) Borst Laboratory. For functional comparisons between the widely used Borst and National Institutes of Health (NIH) MDR1-MDCKII cell lines as well as relevant experimental procedures, see: Feng, B.; West, M.; Patel, N. C.; Wager, T.; Hou, X.; Johnson, J.; Tremaine, L.; Liras, J. Validation of Human MDR1-MDCK and BCRP-MDCK Cell Lines to Improve the Prediction of Brain Penetration. *J. Pharm. Sci.* **2019**, *108*, 2476−2483.

(27) Calculated with the ChemAxon pK_a plugin.

(28) Hopkins, A. L.; Keserü, M. G.; Leeson, P. D.; Rees, D. C.; Reynolds, C. H. The role of ligand efficiency metrics in drug discovery. *Nat. Rev. Drug Discovery* **2014**, *13*, 105−121.

(29) Compound **20e** was dosed orally at 30 mg/kg in mice 2 h prior to brain collection and dissection. The forebrain tissues were homogenized and incubated with ^{3}H-pirenzepine for 10 min. After washing, the residual radioactivity in the forebrain homogenate was quantified and normalized. For an additional application of ^{3}H-pirenzepine, see: Valuskova, P.; Farar, V.; Forczek, S.; Krizova, I.; Myslivecek, J. Autoradiography of ^{3}H-pirenzepine and ^{3}H-AFDX-384 in Mouse Brain Regions: Possible Insights into M_1, M_2, and M_4 Muscarinic Receptors Distribution. *Front. Pharmacol.* **2018**, *9*, 124.

(30) For reported binding affinities (K_i values) of several pan-antimuscarinics across human M_{1-5} receptors, see: Casarosa, P.; Bouyssou, P.; Germeyer, S.; Schnapp, A.; Gantner, A.; Pieper, M. Preclinical Evaluation of Long-Acting Muscarinic Antagonists: Comparison of Tiotropium and Investigational Drugs. *J. Pharmacol. Exp. Ther.* **2009**, *330*, 660−668.

(31) Maeda, S.; Xu, J.; Kadji, F. M. N.; Clark, M. J.; Zhao, J.; Tsutsumi, N.; Aoki, J.; Sunahara, R. K.; Inoue, A.; Garcia, K. C.; Kobilka, B. K. Structure and selectivity engineering of the M_1 muscarinic receptor toxin complex. *Science* **2020**, *369*, 161−167.

https://dx.doi.org/10.1021/acsmedchemlett.0c00626
ACS Med. Chem. Lett. 2021, 12, 155−161